NON-ISOTROPIC MATERIAL DISTRIBUTION TOPOLOGY OPTIMIZATION FOR FUSED DEPOSITION MODELING PRODUCTS

Robert Hoglund and Douglas E. Smith
Department of Mechanical Engineering
Baylor University

Abstract

Mechanical properties of products produced with the Fused Deposition Modeling (FDM) process are known to be dependent on bead direction, especially when short fiber reinforcement is added to the polymer filament feedstock. As a result, the structural performance of fiber-filled FDM parts is expected to be improved by simultaneously computing preferred deposition directions while optimizing the internal support structure. This paper presents a topology optimization method for computing the material distribution within a fiber-reinforced polymer composite FDM part that incorporates the non-isotropic mechanical properties of the bead structure. Unlike the well-established homogenization topology optimization method which determines pointwise orthotropic properties by increasing the complexity of the design problem, our approach takes advantage of the simplicity of the SIMP method where the underlying orthotropic orientation is assumed. Computed results show the effect that the orientation of fiber filled bead orthotropic microstructure has on part topology for 2D FDM parts.

Introduction

The use of Fused Deposition Modeling (FDM) has expanded greatly over the past two decades due in part to its low cost and selection of materials. Unfortunately, the reduced mechanical properties of a typical FDM layered structure must be addressed for this technology to reach its full potential in producing engineering products. The method of extrusion during part processing has been shown to give the final FDM product non-isotropic properties with increased stiffness in the deposition direction [1]. The stiffness and strength of ABS polymer structures produced with FDM has also been shown to improve with the added reinforcement of single-walled carbon nanotubes and short glass fibers [2], [3]. Recently, the effects of carbon fiber content and fiber length have been found to increase the Young's modulus of FDM parts to varying degrees [4], increasing the modulus of elasticity by as much as 4X in the print direction.

Topology optimization has been shown to be an effective tool for the design of structures produced with additive manufacturing where an optimal material distribution in a design domain is determined for a given material volume [5], [6]. Topology optimization is commonly performed to maximize the stiffness of a part while retaining a given fraction of material volume in the design domain. The Homogenization Method was developed to determine an optimal material distribution and orthotropic material orientation distribution within a structure [7]. Unfortunately, the homogenization method, as well as SIMP methods that have been extended to include pointwise material orientation as part of the design problem [8], is impractical to implement in FDM, as it is not possible to produce a part where each point within the structure has a unique material direction. An alternative approach, the SIMP (Solid Isotropic Material with Penalization) method [9], or density method [10], computes material distributions for isotropic materials. The SIMP method has seen extensive use in additive manufacturing where

888

unique three dimensional microstructures designed for a prescribed mechanical response are printed with additive manufacturing methods (see e.g., Hollister, et al., (2003)) [11]. More recently, the distribution of varying microstructure has been computed with a modified SIMP method where the printed optimal design includes the details of optimal unit cell geometries (see e.g., Sundararajan (2010) and Zhang, et al., (2015)) [12], [13]. This latter research computes the effective orthotropic material matrix for a unit cell having varying density which serves as the design variable in the topology optimization. Alamo and da Silva (2012) extended the SIMP method to compute a material distribution for a fixed orthotropic material distribution in a biomechanics structure [14].

FDM offers a unique advantage in that beads of material having a preferred orientation can be deposited in nearly any desired orientation. Unfortunately, to the best of our knowledge, design tools to date have not addressed the topology optimization problem for a predefined underlying orthotropic material for the FDM process. This paper considers a modified SIMP approach that determines the optimal distribution of an orthotropic material with fixed material orientation to design fiber-reinforced FDM parts.

Two-dimensional Orthotropic Model for Fused Deposition Modeling

In this work, a topology optimization method for linear elastic orthotropic materials is implemented in MATLAB using the framework developed by Sigmund [15]. Previous studies that focused on orthotropic materials using the homogenization method optimized both material orientation and distribution within a design domain. Rather than optimizing the orientation of material at each point as in the homogenization method, the present work assumes the underlying orientation of the material and the related elastic properties are known and thus are not part of the design problem. To this end the SIMP method is modified with the goal of direct application to FDM deposition of optimal structures. The optimization problem formulated for minimization of compliance c of a statically loaded structure analyzed with the finite element method is [15]

$$min: \ c(\boldsymbol{x}) = \ \boldsymbol{U}^T \boldsymbol{K} = \ \sum_{e=1}^{N} (x_e)^p u_e^T k_0 u_e$$

$$s.t.: \ \frac{V(x)}{V_0} = f, \quad \boldsymbol{KU} = \boldsymbol{F}, \quad 0 < x_{min} \leq x \leq 1$$

(1)

where the x_e are elemental densities that form the design variable vector $\boldsymbol{x}$, u_e are elemental nodal displacements, and k_0 is the elemental stiffness matrix. The penalization parameter p is used to penalize intermediate element densities by driving them towards 0 or 1. The SIMP topology optimization is constrained by a predefined volume fraction f, which is equated to the sum of element volumes $V(\boldsymbol{x})$ divided by the total volume V_0 where each elemental volume is scaled by its respected element density x_e. A finite element analysis of the structure is performed to evaluate nodal displacements $\boldsymbol{U}$, where $\boldsymbol{K}$ is the global stiffness matrix and $\boldsymbol{F}$ the nodal force vector. To avoid matrix singularities while solving the finite element system of equations, the lower limit on the design variables is set to $x_{min} = 0.001$.

In the topology optimization problem, each element is assigned an independent elemental density, which collectively compose the design variables of the optimization problem. In our simulations, design variables are updated as in Sigmund [9] based on design sensitivities

computed with the Adjoint Variable Method as the derivatives of the objective function and constraints with respect to the design variable vector. A density filter is implemented in the update of the elemental densities to reduce the well-known checkerboarding effect [16]. The optimization problem is solved to minimize the compliance using an optimality criteria (OC) method with a predefined move limit. In the SIMP method, the modulus of elasticity for each element is defined as a function of the related elemental density with $p = 3$, which tends to cause an element to vanish (i.e., the element density becomes zero) or cause it to become fully solid (i.e., the element density becomes unity).

Topology optimizations solved with the SIMP method assumes that elements in the model are composed of an isotropic elastic material. In this paper, the SIMP method is modified such that the material in each element is orthotropic elastic. The resulting topology optimization which scales the predefined elemental elasticity matrix with the element density is designated as the SOMP method (Solid Orthotropic Material with Penalization) as in [14]. For plane stress, the 2D elasticity matrix derived from Hooke's Law is given as

$$D = \begin{bmatrix} \dfrac{E_x}{1 - v_{xy}v_{yx}} & \dfrac{v_{yx}E_x}{1 - v_{xy}v_{yx}} & 0 \\[3mm] \dfrac{v_{yx}E_x}{1 - v_{xy}v_{yx}} & \dfrac{E_y}{1 - v_{xy}v_{yx}} & 0 \\[3mm] 0 & 0 & \dfrac{E_x}{2(1 + v_{xy})} \end{bmatrix} \tag{2}$$

The elemental stiffness matrix k_0 in equations (1) is defined as the integral

$$k_0 = \int_{A_e} B^T D B \; dA \tag{3}$$

where B is the strain-displacement matrix and the integration is performed over the element domain A_e. In equation (2), E_x and E_y are the Young's modulus in the x- and y- directions, respectively, and v_{xy} and v_{yx} are the Poisson's ratios in the x-y plane. The ratio between Young's modulus and Poisson's ratio in respective directions, due to the required symmetry of the compliance matrix, is

$$\frac{E_x}{v_{yx}} = \frac{E_y}{v_{xy}} \tag{4}$$

It is important to note that in our approach, the elastic properties and material orientation are defined apriori and remain fixed throughout the optimization. The fixed elemental elasticity matrix D is simply scaled by the elemental density x_e in the compliance calculation of equation (1) during the optimization to obtain the desired result. Our implementation is simplified by considering only square element of unity length on a side to yield a closed form solution for the integral that defines k_0 in equation (3). In addition, the direction of orthogonal orientation may be rotated through an angle theta formed with x-axis with

$$D' = RDR^T \qquad (5)$$

where R is a rotation matrix about the z- axis:

$$R = \begin{bmatrix} \cos(\theta) & -\sin(\theta) & 0 \\ \sin(\theta) & \cos(\theta) & 0 \\ 0 & 0 & 1 \end{bmatrix} \qquad (6)$$

The resulting element stiffness matrix for an orthotropic material aligned as specified by the angle theta is given as

$$k_0 = \int B^T RDR^T B \, dA_e \qquad (7)$$

The stiffness matrix in equation (7) in the finite element analysis of equation (1) allows for both varying Young's modulus and Poisson's ratios in two orthogonal directions, as well as a rotation of the properties throughout the material distribution by a specified angle. Implementing this in the existing topology optimization structure yields a simple, yet effective two-dimensional model for determining the material distribution of solid-filled two-dimensional FDM parts with the inclusion of desired boundary conditions on the design domain. It must be stressed, however, that the optimization model determines optimal material orientation for stiffness, not part strength, and as such, the optimized orthotropic models should not be necessarily expected to have a higher yield strength than those predicted by the isotropic topology optimization.

Computational Results

In order to show the applicability of the orthotropic model to FDM part design, several tests of the 2D model are shown, using the Messerschimitt-Bölkow-Blohm (MBB) beam and the Michell truss [17]. Two-dimensional versions of these beam designs are implemented with a varying range of conditions to compare these optimal structures with those obtained assuming an isotropic SIMP model. In addition to adding orthotropic properties to the topology optimization model, the code has been vectorized to improve the speed of the finite element analysis calculations significantly as in [18]. It is worth noting the simplicity of this approach; modifying the construction of the elemental stiffness matrices is a simple way to model a layer of a carbon fiber-reinforced FDM part, assuming that certain material properties, such as Young's modulus and Poisson's ratio of the material are known.

First, in order to test the validity of the orthotropic modifications against the original isotropic SIMP model, optimizations are performed with our orthotropic code using isotropic material properties for comparison with isotropic code results. Our model runs identically to the isotropic case, solving it with same topology in the same number of iterations. Young's modulus is defined as an initial unit of 1 Pa in both directions for the purpose of illustrational ease. Poisson's ratio of the major direction (greater Young's modulus) is defined to be 0.36, an approximate ratio for polylactic acid (PLA) polymer-printed structures, and $p = 3$. The topology optimization scheme iterates until the greatest change in elemental density is less than 1%.

The MBB beam is a truss-like structure popularized in many topology optimization studies. In the following optimizations, a design domain of 601 by 100 elements is discretized, with a prescribed volume fraction of 50%. The design domain is set to be fixed vertically at the bottom corner nodes with a load applied downward at the top of the center. Figure 1 shows the result of the topology optimization with Young's Modulus equal in both orthogonal directions, equivalent to the isotropic case.

Figure 1: Full MBB beam, isotropic case ($E_x = E_y$)

It is worth noting that the developed microstructure of the isotropic case is symmetric. To demonstrate the orthotropic properties of the material, the Young's modulus is increased in one direction only by a magnitude of 10. Figures 2 and 3 show the resulting material distributions produced by the topology optimizations where, respectively, E_y and E_x are increased by 10x in separate optimizations.

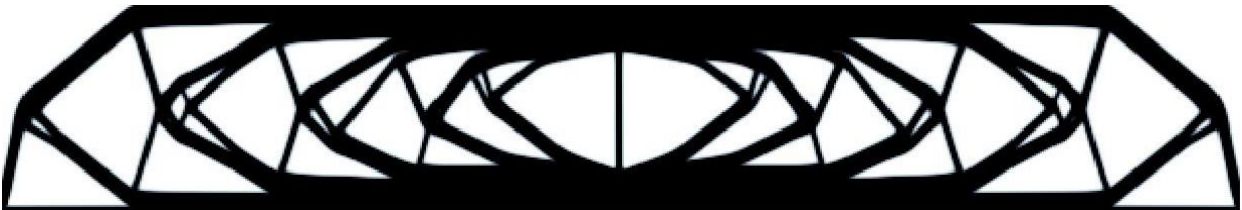Figure 2: Full MBB beam, E_y increased 10x

Figure 3: Full MBB beam, E_x increased 10x

With this variation in orthotropic properties, it is apparent that an increase in Young's modulus by an order of magnitude leads to a sufficient change in material distribution of the part. When the value of Young's modulus is increased significantly in the y- direction, for instance, the solution design provides more directional reinforcement at an angle that is nearer to the direction of increased modulus. Likewise, the directional reinforcement along the x- axis increases greatly when the Young's modulus in that direction is an order of magnitude greater.

The optimal topologies are characterized by thick reinforcement near the top and bottom of the beam. This reinforcement spreads the load out along the width of the MBB beam to the bottom corner nodes. In some areas of the microstructure for these examples, there are areas of thinner reinforcement similar to the isotropic model. However, the fact that thinner areas of reinforcement are typically oriented more in the direction of higher Young's modulus is an expected artifact of the orthotropic material properties employed in the finite element analysis.

Figure 4 shows the effect of additional reinforcement in the y- direction by a factor of 1.35, which is more realistic of a layer of carbon fiber-reinforced plastic extruded by FDM. There is still a noted difference in the resulting topology as compared with the isotropic case, indicating that the physical modeling of orthotropic materials more accurately determines optimal FDM material distribution than isotropic models. Likewise, Figure 5 shows the increased elastic modulus in the x- direction by a factor of 1.35.

Figure 4: Full MBB beam, E_y increased 1.35x

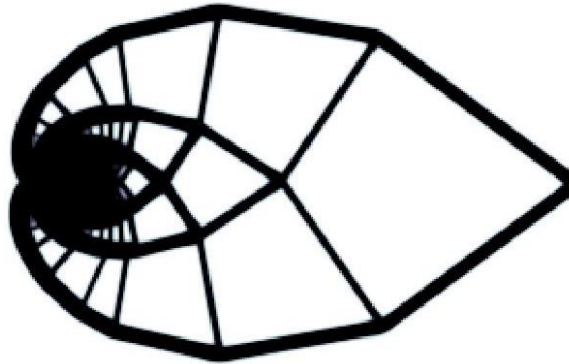

Figure 5: Full MBB beam, E_x increased 1.35x

Compliance minimization values for the optimization cases noted are shown in Table I. Compliance is assumed to be calculated as the inverse of stiffness for this study as the load is set to be equal to 1 N. Stiffness values are shown alongside compliance for the structures. Interesting to note is the fact that an increase in E_y has a minimal increase in stiffness of the MBB beam, whereas an increase in E_x has a much more profound effect on stiffness.

Table I: Compliance and Stiffness Values for Orthotropic MBB Beam Topology Optimizations

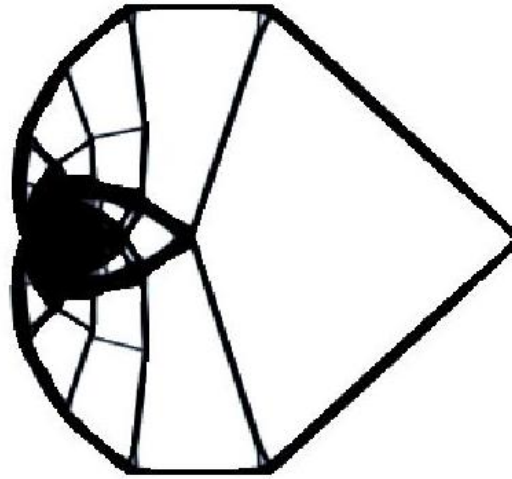| MBB Young's Modulus Ratio	Minimum Compliance (N·m)	Maximum Stiffness (N/m)
1 x : 1 y (Isotropic)	94.25	0.011
10 x : 1 y	13.82	0.072
1 x: 10 y	82.70	0.012
1.35 x: 1 y	71.83	0.014
1 x: 1.35 y	91.57	0.011

In addition to the MBB beam, the Michell truss is also optimized with varying orthotropic material properties. The Michell truss features a set of fixed points, often in a circle, at a location interior to the design domain on its left side, with a downward force at the right center of the design domain. Here, four fixed points, spaced at a distance 1/6 of the distance along the length of the domain, are chosen centered in the vertical direction. Studies of this structure are computed with a design domain of size 300 by 250 elements, with a fixed volume fraction of 15%. Figure 6 shows the computed isotropic topology for the Michell truss.

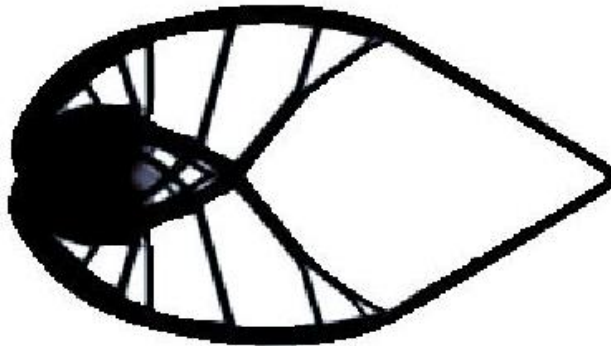Figure 6: Michell Truss, isotropic case

The resulting material distribution of the Michell truss is concentrated near the fixed nodes. The effects of orthotropic material properties on material distribution are observed and shown in Table II. Figure 7 shows the resulting material distribution produced by an increase in Young's modulus in the y-direction by a factor of 2.

Figure 7: Michell Truss, y-modulus increased 2x

As before, the directional reinforcement is much more pronounced vertically than the isotropic case. Certain horizontal reinforcements that were present in the isotropic topology optimization have either disappeared, faded, or have simply shrunk in size. The reinforcement pushes to the vertical boundaries of the design domain. Likewise, Figure 8 shows the effects of increased Young's modulus in the horizontal direction.

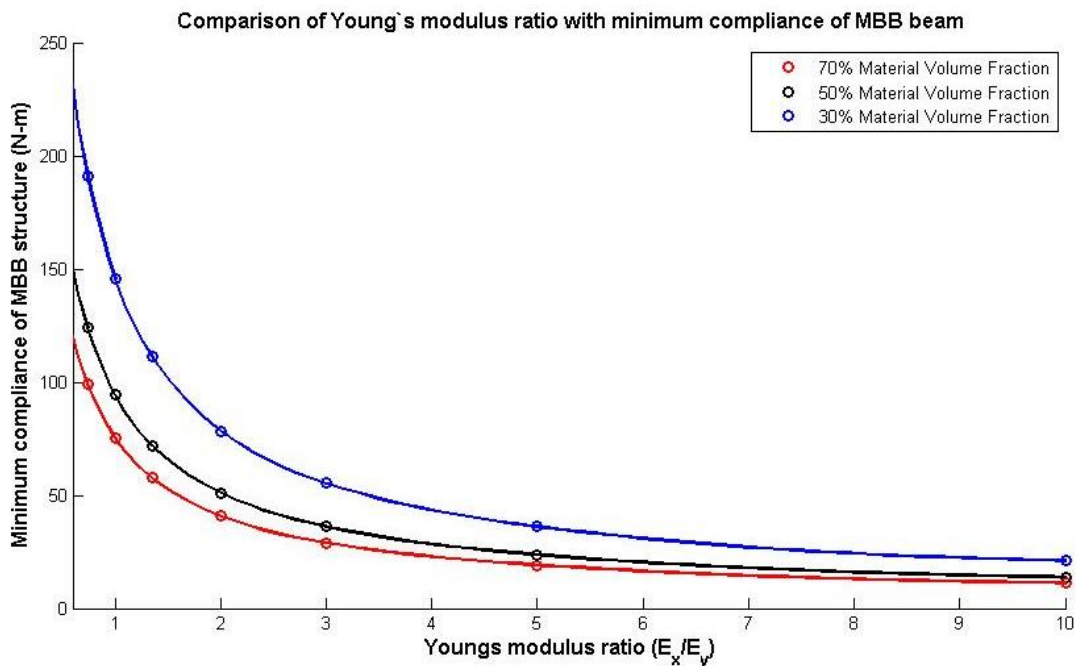Figure 8: Michell Truss, x-modulus increased 2x

The structural reinforcement appearing in Figure 8 in the x-direction is thicker, due to the defined increased stiffness in this direction. The Michell truss is not as thick vertically due to the relative decrease in elastic modulus in this direction. Table II shows a comparison of compliance and stiffness between these structures.

Table II: Compliance and Stiffness Values for Orthotropic Michell Truss Topology Optimizations

Michell Truss Young's Modulus Ratio	Minimum Compliance (N·m)	Maximum Stiffness (N/m)
1 x : 1 y (Isotropic)	27278.38	$3.67*10^{-5}$
2 x : 1 y	15085.24	$6.63*10^{-5}$
1 x: 2 y	22005.29	$4.54*10^{-5}$

To further explore the effect of optimal topologies on the directional properties of the underlying material, additional simulations were performed on the MBB beam with varying orthotropic material values. In addition to the physical change in the design domain, the effects of changing ratio of Young's modulus and material distribution upon minimum structural compliance for the MBB beam are explored. The minimum compliance of the MBB beam as calculated by the model for a variety of ratios and material volume fractions are shown in Figure 9. Here, the minimum compliance of the MBB beam is plotted as a function of the ratio of Young's modulus in the horizontal direction to the vertical direction. The Poisson's ratio in the horizontal direction is held constant again at 0.36, and Young's modulus in the vertical direction set as an arbitrary value of 1.

Figure 9: Parametric Study of MBB Beam

As the ratio of Young's modulus increases in the horizontal direction (i.e., E_x increases), the minimum compliance of the computational model decreases, indicating an inverse relationship as expected. It is also true that an increase in volume fraction in the material distribution decreases the minimum compliance for all Young's modulus ratios, and a decrease in volume fraction will increase the minimum compliance for all ratios.

Finally, a method of multi-material orthotropic topology optimization is developed for considering varying properties in FDM on a domain. In this work, most important is the effect of Two sets of orthotropic properties are proposed and split in two even areas on the domain. The inclusion of continuum orthotropic properties is accomplished through the use of a single elemental stiffness matrix k_0. However, in order to demonstrate the usefulness of the method, the design domain can be broken up into multiple sections with varying orthotropic properties

and the topology optimization performed. The formulation of the optimization problem then changes slightly in the compliance calculation and finite element analysis:

$$min: \ c(x) = \ U^T K = \sum_{i=1}^{N_1} (x_i)^p u_i^T k_1 u_i + \sum_{j=1}^{N_2} (x_j)^p u_j^T k_2 u_j \tag{8}$$

where k_1 and k_2 are separate elemental stiffness matrices, N_1 and N_2 are, respectively, the number of elements on the zones 1 and 2 of the design domain. Similarly, x_i and x_j are the elemental densities for the zones 1 and 2 of the design domain, respectively. Loop vectorization is used to keep computational time as low as possible for each iteration. In the finite element analysis, two different elemental stiffness matrices k_1 and k_2 are calculated based on their respective elemental properties and assembled in the global stiffness in the usual manner. The respective compliance values, physical elemental densities and design sensitivities are then calculated and summed. Figure 10 shows the design domain split into thirds, with two zones of orthotropic properties. Figure 11 shows the solution of the multi-orthotropic model with properties in zone I having reinforcement in the vertical direction $E_y =1$, $E_x = 10$, and properties in zone II of $E_x = 1$, $E_y = 10$. Figure 12 shows the same optimization, but with the material properties of the zones reversed.

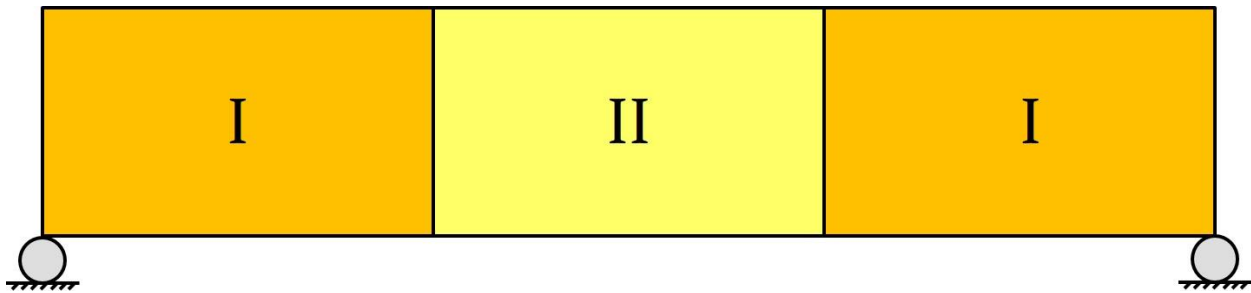Figure 10: Multi-zone topology optimization

Figure 11: 3-zone orthotropic topology optimization, zone I horizontal, zone II vertical
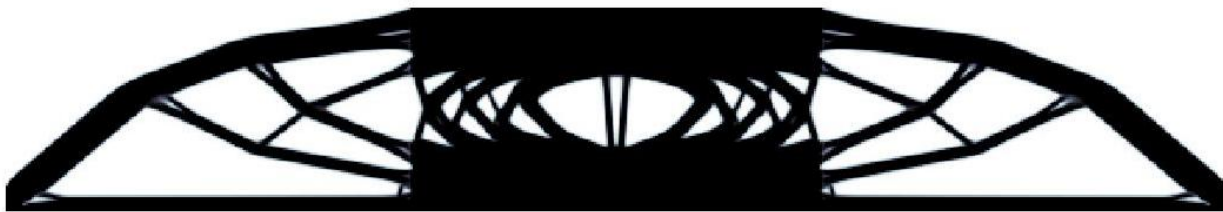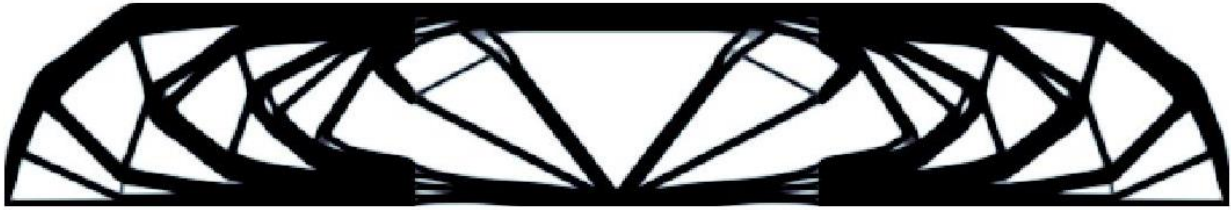
Figure 12: 3-zone orthotropic topology optimization, zone I vertical, zone II horizontal

The material distribution of the beam in Figure 11 in the left and right regions is comparable to the same thickened arch reinforcement of the MBB beam that was optimized entirely in the horizontal direction (Fig. 3). However, the center of the beam exhibits some structural similarities to the vertically reinforced beam in pushing the material distribution to the top and bottom. In Figure 12, the layout is consistent with that of the vertically optimized beam (Fig. 2), except in zone II, where the material is weak in the vertical direction. These results show the ability of topology optimization to predict correct material distribution for varying print orientations of non-isotropic carbon-fiber reinforced polymers. The computational results demonstrate the high importance of varying orthotropic material properties in determining the correct distribution of the material topology, as well as the maximum stiffness of resulting printed structures.
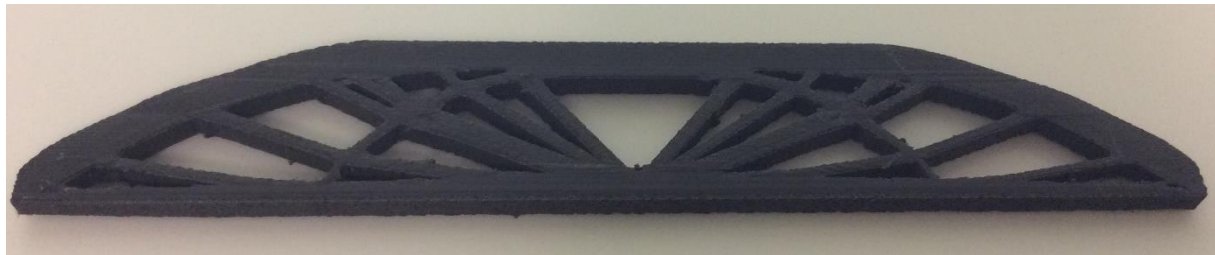
Experimental Setup

In order to demonstrate the usefulness of the method, full MBB beams are printed with varying orientations using carbon fiber-reinforced PLA (3DxTECH). The filament contains approximately 20% carbon fibers by weight in a 1.77 mm diameter filament. For FDM processing, MBB structures are produced with a MakerBot Replicator 2.0 printer with a standard 0.4 mm nozzle size. The Young's Modulus and Poisson's ratios of the topology optimized structures are computed with a fixed directional modulus ration having an order of magnitude difference as before to highlight the effect of orthotropic properties on maximum stiffness of the structure, as well as solution microstructure.

To produce a printable format of the topology optimizations, the code `Top3dSTL_v3.m` was used to convert the physical array of elemental densities to .stl file format [19]. The resulting files were then exported using MakerBot Desktop property settings and printed. As in the computations above, a 50% material distribution throughout the design domain was chosen, as very thin structures that could not be printed accurately were not desired to be tested. Parts were printed with a solid, linear fill with the major bead direction pertaining to the direction of the computational model's increased Young's modulus and a layer thickness of 0.2 mm. A single shell is printed for each layer. The shell layer is expected to have some effect upon the material properties in testing as this shell is not printed in the vertical or horizontal orientation as defined in the topology optimization results.

The goal of testing is to show the effectiveness of compliance minimization in relation to the build orientations developed through the topology optimization model. A straightforward method to determine the usefulness of the orthotropic model involves the printing and testing of

structures proposed with clear sets of orthotropic properties. Two samples are printed: Orthotropic horizontally reinforced with horizontal bead direction, orthotropic vertically reinforced with vertical bead direction. For the purpose of the test, the models are printed with a uniform bead direction (except for the shell layer as mentioned above). Figure 12 shows the printed structures.

Figure 12: Printed MBB Structures

A) Orthotropic horizontal distribution, printed in the horizontal direction

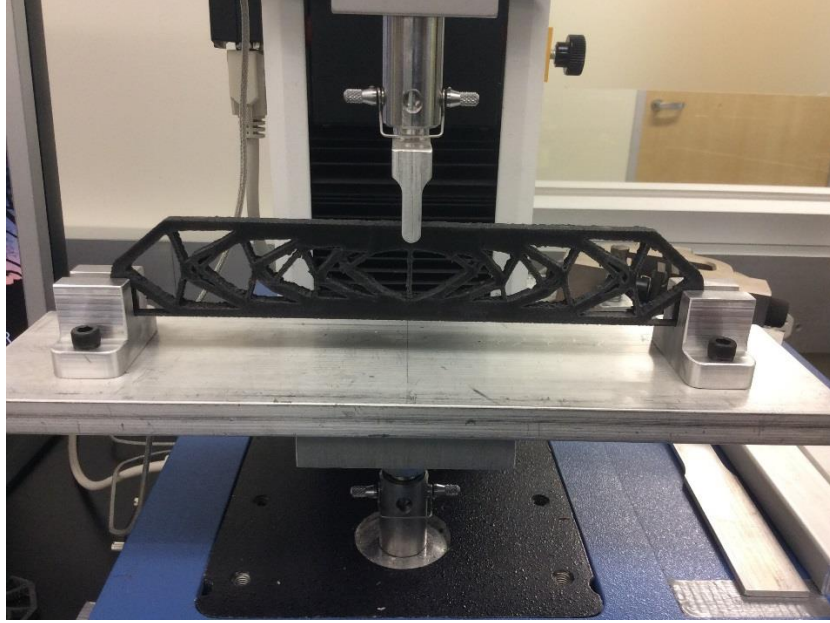B) Orthotropic vertical distribution, printed in the vertical direction

The MBB structures are weighed and results reported in Table III. There is some variation due to the print direction, although all parts were printed at 50% of the fixed volume region.

Table III: Carbon Fiber MBB-Beam Weight

MBB Beam	Weight (g)
Orthotropic in x-direction, printed in horizontally	26.98
Orthotropic in y-direction, printed vertically	28.29

The stiffness of each truss is determined using an INSTRON 2-kN loading machine via a 3-point bend test. A test fixture was machined with a 1/2" aluminum base plate and fixtures that contain slots to allow the MBB beam structure to move horizontally, but sit upright during the test as a load is applied. The test setup is shown in Figure 13.

Figure 13: Test Setup for MBB Beam Samples

A load is applied at the center of the top of the beam in a compression test. The goal is not to test structures to failure. By recording the slope of the linear portion of the load-displacement curve, the stiffness of the structure is determined. Structures are tested at a rate of 1 mm/min to determine the linear relationship between load and displacement and pushed to an extension near 2.5 mm.

Experimental Results

Since the ratio of the Young's modulus for carbon-reinforced PLA is estimated in the topology optimization model, it is expected that there will be some deviation between the calculated optimal material distribution and the actual optimal material distribution of the printed sample. However, the inclusion of orthotropic material continuum in the model produces a significant change in topology given the fact that Young's modulus of FDM-produced layers is higher along the bead direction than the orthogonal direction. Figure 14 shows the load-displacement curve of the parts that are printed in the horizontal and vertical directions with given orthotropic properties.

The stiffness of the part printed and optimized in the horizontal direction is slightly higher than the stiffness of the part printed and optimized in the vertical direction. This is attributed to the orthotropic material properties relative to the vertical loading condition. A linear regression is used to determine the linear elastic region of the sample curves, with a calculated correlation coefficient of $R > 0.99999$ for each curve. Table IV shows the calculated stiffness of the MBB samples.
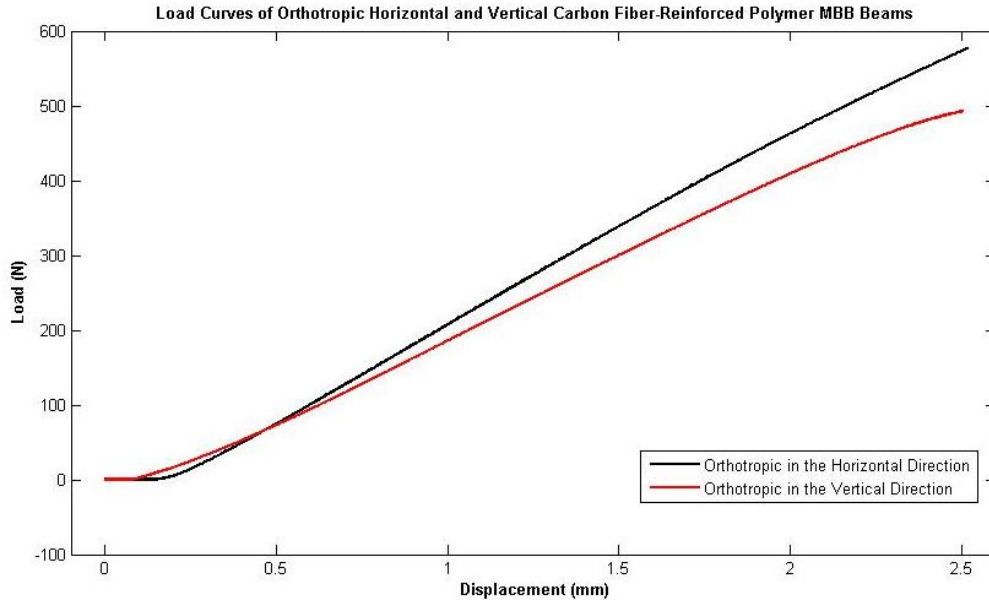
Figure 14: Load Curves

Load Curves of Orthotropic Horizontal and Vertical Carbon Fiber-Reinforced Polymer MBB Beams

Table IV: Relative Stiffness Values of Varying MBB Beams

MBB Beam	Experimental Stiffness (N/m)	Scaled Model Stiffness (N/m) 1.35 x	Scaled Model Stiffness (N/m) 10 x
Orthotropic X	$2.66*10^5$	$7.70*10^4$	$3.96*10^5$
Orthotropic Y	$2.29*10^5$	$6.05*10^4$	$6.6*10^4$

The horizontally reinforced beam has a higher stiffness than the vertically reinforced beam, which is also true in the computational results shown in Table I, showing the effect of orthotropic properties on the beam structure. The ratio between the beams reinforced by a factor of 1.35 is closer to the experimental results than the factor of 10 scaled model, indicating that for this carbon fiber PLA filament, the increase in modulus along the bead direction is closer to a factor of 1.35, as expected. The evidence of directional dependence in the topology optimization results is indicative of a further application for topology optimization in FDM, specifically with short fiber-reinforced polymers, which make structurally designed parts more viable for practical applications.

Conclusions and Future Work

A method for topology optimization of 2D structures has been developed with regards to materials which exhibit varying measures of strength in two orthogonal directions and specifically for carbon fiber-reinforced FDM products. The stiffness of the structures are maximized for a particular volume fraction given the boundary conditions, and computed results agree with the isotropic model computed by the SIMP method in previous works. There is

significant variance in structural topology exhibited by the orthotropic model solutions, depending on the direction of increased Young's Modulus. This method provides a basis for which topology optimization of FDM produced parts can be produced given the orthotropic nature of the printed products.

Future work includes further testing of optimized structures when printed in the correct orientation, and the carbon-fiber reinforced PLA offers a distinct advantage for the production of stiff parts, such as supports and trusses, for commercial applications. In order to better model the orthotropic properties, more data needs to be determined on the Poisson's ratios and Young's modulus of carbon fiber-reinforced PLA in printed FDM parts. These can then be easily implemented with the topology optimization model to improve solution accuracy. The inclusion of an orthotropic filter based on the orthotropic nature of the material will also be investigated. Ultimately, the goal is to extend orthotropic prediction properties to a 3D model, where a certain number of layers of polymer bead are modeled by a layer of hexahedral elements. Thus, the orthotropic properties of the material can be modeled with a three dimensional structure for a more practical application to FDM. Plans for the addition of an additional overhang constraint to the topology optimization routine will restrict the design domain to feasible designs for the FDM process. Additionally, FDM modeling of 3D carbon-fiber reinforced structures will be experimentally tested to show improved stiffness in the desired build orientations.

Acknowledgements

References

[1] A. Bellini and G. Selcuk, "Mechanical characterization of parts fabricated using fused deposition modeling," *Rapid Prototyp. J.*, vol. 9, no. 4, pp. 252–264, 2003.

[2] M. L. Shofner, K. Lozano, F. J. Rodríguez-Macías, and E. V. Barrera, "Nanofiber-reinforced polymers prepared by fused deposition modeling," *J. Appl. Polym. Sci.*, vol. 89, no. 11, pp. 3081–3090, Sep. 2003.

[3] W. Zhong, F. Li, Z. Zhang, L. Song, and Z. Li, "Short fiber reinforced composites for fused deposition modeling," *Mater. Sci. Eng. A*, vol. 301, pp. 125–30, 2001.

[4] W. C. Fuda Ning, "ADDITIVE MANUFACTURING OF CFRP COMPOSITES USING FUSED DEPOSITION MODELING: EFFECTS OF CARBON FIBER CONTENT AND LENGTH," 2015.

[5] H. de A. Almeida and P. J. da Silva Bártolo, "Virtual topological optimisation of scaffolds for rapid prototyping," *Med. Eng. Phys.*, vol. 32, no. 7, pp. 775–782, Sep. 2010.

[6] N. P. Fey, B. J. South, C. C. Seepersad, and R. R. Neptune, "Topology Optimization and Freeform Fabrication Framework for Developing Prosthetic Feet," presented at the Solid Freeform Fabrication Symposium, University of Texas at Austin, 2009.

[7] M. P. Bendsoe, "Generating optimal topologies in structural design using a homogenization method," *Comput. Methods Appl. Mech. Eng.*, vol. 71, no. 2, pp. 197–224, 1988.

[8] H. P. Jia, C. D. Ling, G. P. Li, R. Q. Mu, and C. B. Jiang, "Topology Optimization of Orthotropic Material Structure," *Mater. Sci. Forum*, vol. 575–578, pp. 978–989, Apr. 2008.

[9] M. P. Bendsøe, "Optimal shape design as a material distribution problem," *Struct. Optim.*, vol. 1, no. 4, pp. 193–202, Dec. 1989.

[10]   R. J. Yang and C. H. Chuang, "Optimal topology design using linear programming," *Comput. Struct.*, vol. 52, no. 2, pp. 265–275, Jul. 1994.

[11]   J. M. Taboas, R. D. Maddox, P. H. Krebsbach, and S. J. Hollister, "Indirect solid free form fabrication of local and global porous, biomimetic and composite 3D polymer-ceramic scaffolds," *Biomaterials*, vol. 24, no. 1, pp. 181–194, Jan. 2003.

[12]   V. Sundararajan, "Topology Optimization for Additive Manufacturing of Customized Meso-Structures using Homogenization and Parametric Smoothing Functions," MS, University of Texas at Austin, 2010.

[13]   P. Zhang, J. Toman, Y. Yu, E. Biyikli, M. Kirca, M. Chmielus, and A. C. To, "Efficient Design-Optimization of Variable-Density Hexagonal Cellular Structure by Additive Manufacturing: Theory and Validation," *J. Manuf. Sci. Eng.*, vol. 137, no. 2, pp. 021004–021004, Apr. 2015.

[14]   J. Alamo and F. da Silva, "Adapting the SIMP Model for Topology Optimization of Biomechanical Structures," presented at the 12th Pan-American Congress of Applied Mechanics - PACAM XII, 2012.

[15]   O. Sigmund, "A 99 line topology optimization code written in Matlab," *Struct. Multidiscip. Optim.*, vol. 21, no. 2, pp. 120–127, Feb. 2014.

[16]   O. Sigmund and J. Petersson, "Numerical instabilities in topology optimization: A survey on procedures dealing with checkerboards, mesh-dependencies and local minima," *Struct. Optim.*, vol. 16, no. 1, pp. 68–75, Aug. 1998.

[17]   A. Michell, "The limits of economy of material in frame structures," *Philos. Mag.*, vol. 8, no. 47, pp. 589–597, 1904.

[18]   E. Andreassen, A. Clausen, M. Schevenels, B. S. Lazarov, and O. Sigmund, "Efficient topology optimization in MATLAB using 88 lines of code," *Struct. Multidiscip. Optim.*, vol. 43, no. 1, pp. 1–16, Nov. 2010.

[19]   K. Liu, "Top3dSTL_v3," *Top3d: An Efficient 3D Topology Optimization Program*, Apr-2015. [Online]. Available: https://top3dapp.com/download-archive/. [Accessed: 04-Aug-2015].